Materials Science and Engineering C 59 (2016) 773–781

Contents lists available at ScienceDirect

Materials Science and Engineering C

journal homepage: www.elsevier.com/locate/msec

Synergistic effect of magnetite and gold nanoparticles onto the response of a label-free impedimetric hepatitis B virus DNA biosensor

Mohammad Hossein Mashhadizadeh, Rasoul Pourtaghavi Talemi *

Faculty of Chemistry,Kharazmi University,Tehran,Iran

ARTICLE INFO

Article history:
Received 3 May 2015
Received in revised form 8 October 2015
Accepted 26 October 2015
Available online 28 October 2015

Keywords:
Carbon paste electrode,
Impedimetric DNA biosensor,
Hepatitis B virus,
Gold nanoparticles,
Magnetic nanoparticles,
Label free

ABSTRACT

A magnetite and gold nanoparticle modified carbon paste electrode (CPE) was prepared for the immobilization of a thiol modified Hepatitis B virus (HBV) probe DNA and determination trace amount of target HBV DNA. Indeed, the sensing platform integrated two nanoparticles that had previously been employed individually in the DNA biosensors. The proposed DNA biosensor could measure target HBV DNA virus concentration with a low detection limit of 3.1 ($\pm$0.1) $\times$ 10–^{13} M, which was greatly lower than the detection limit reported with gold or magnetite nanoparticles alone. The change of interfacial charge transfer resistance (R_{CT}) was confirmed the hybrid formation between probe and target HBV DNA. The R_{CT} difference (before and after hybridization with the target HBV DNA) was in a linear relationship with the logarithm of complementary oligonucleotide concentrations in the range of 8.3 ($\pm$0.1) $\times$ 10^{-13} to 6.4 ($\pm$0.2) $\times$ 10^{-7} M. In addition, the novel methodology for specific DNA sequence detection was highly selective, repeatable, and reproducible. Finally, this work was successfully utilized for the sensitive and label free impedimetric determination of HBV target DNA in the urine and blood plasma samples.

1. Introduction

Viral hepatitis due to hepatitis B virus (HBV) is a major public health problem all over the world. Hepatitis B is a complex virus, which replicates primarily in the liver, causing inflammation and damage, but it can also be found in other infected organs. For this reason, the hepatitis B vaccine is strongly recommended for health-care workers, people who live with someone with hepatitis B, and others at higher risk. In many countries, hepatitis B vaccine is inoculated to all infants, and it is also recommended to previously unvaccinated adolescents [1,2].

The determination of specific DNA sequences provides the basis for detecting a wide variety of microbial and viral pathogens. Traditional methods for DNA sequencing, based on the coupling of electrophoretic separations and radio-isotopic (^{32}P) detection, are labor and time consuming. Electrochemical hybridization biosensors for the detection of DNA sequences may greatly reduce the assay time and simplify its protocol. Such fast on-site monitoring schemes are required for quick preventive action and early diagnosis [3].

Carbon paste electrodes (CPEs) are one of the most commonly used electrodes in the electrochemical investigations. The application of CPEs in analytical chemistry has attracted considerable attention in recent years [4–8].

Although the initial application of electricity to biological materials goes back to the first experiments of Luigi Galvani [9], it has been only recently that the coupling of electrochemistry and biology has resulted in a synergistic field of science, i.e., bioelectrochemistry. The field is growing rapidly and is beginning to have a significant impact on the practice of medicine [10], biology [11], pollution control, energy conversion, food technology, and other areas. Among the facets of bioelectrochemistry that are being investigated are mechanisms of electron transfer by enzymes and other macromolecules, electrochemically stimulated tissue and bone growth, electrical homeostasis, uses of biologically active molecules and organisms in combination with electrodes, and many more [12].

Electroanalytical chemistry can play a very important role in the protection of our environment [13]. In particular, electrochemical sensors and detectors are very attractive for on-site recording of priority pollutants, as well as for addressing other environmental needs. Such devices satisfy many of the requirements for on-site environmental analysis. They are inherently sensitive and selective towards electroactive species, fast and accurate, compact, portable and inexpensive. Such capabilities have already made a significant impact on decentralized clinical analysis [14].

In electrochemical DNA biosensors, detection is based on the variation in the electrical properties of the DNA modified electrode before and after hybridization, which may be due to the change of double-layer capacitance, electronic transfer resistance, impedance or current. In most of the DNA biosensors which produce either electrical or photonic signals, the probes are either modified by electrochemically active

* Corresponding author.
E-mail addresses: rasoulpourtaghavi@gmail.com, rasoulpourtaghavitalemi@yahoo.com (R.P. Talemi).

http://dx.doi.org/10.1016/j.msec.2015.10.082
0928-4931/

substances or labeled; which includes, organic dyes, metal nanoparticles, thiol-linked, enzyme labeled, Biotin labeled, fluorescent and radioactive labeled probes [15,16]. Although, these indirect (labeled) methods proved to be effective, they are complex, expensive, time-consuming, and also may cause DNA damage which in turn affects the DNA recognition. Thus, the direct or the label-free DNA biosensor has become extremely beneficial and can be readily employed for the real-time detection.

Electrochemical impedance spectroscopy (EIS) detection has enabled simplification of the detection and enhancement of the sensitivity of the measurement. EIS recently has been chosen as a main detection method because it has some important advantages over a number of electrochemical methods such as amperometry and potentiometry [12]. As it is known, EIS is an electrochemical technique that provides the examination of electrical properties of electrode surface and binding kinetics of molecules between electrolyte and electrode surface. Therefore, it can be used for biomolecular recognition, biomolecular bindings and biomolecular interactions between molecules such as DNA–DNA, DNA–protein, receptor–ligand, protein–ligand, antibody–antigen, and ion channels–ligands. As a consequence, EIS provides label-free detection without chemical transformation, and most of the bimolecular events can be monitored by EIS expeditiously [17–20].

Due to their small size (1–100 nm), nanoparticles exhibit novel material properties that differ considerably from those of the bulk solid-state [21]. Especially in recent years, the interests in nanometer-scale magnetic particles are growing [22,23]. However, as the particle size decreases, the reactivity of the particle increases and the magnetic properties are influenced more by surface effects [24].

Magnetic nanoparticles (MNP) are a valuable class of nanomaterials with unique properties that remain distinct from those that manifest their bulk counterparts. MNPs typically are in the size range from a few nanometers up to tens of nanometers, which places them at dimensions that are smaller or comparable to those of biological entities, such as cells and proteins. As the magnetic particle size descends from the micron scale to the 10–20 nm size range, the magnetic properties pass from the multi-domain state through higher co-reactivity single-domain regime to the super-paramagnetic regime [25].

Gold and iron oxide magnetic nanoparticles have attracted particular attention and are considered as excellent candidates for surface functionalization because they are easily synthesized, biocompatible, and have a greater surface area. Furthermore, the use of thiol chemistry on the gold surface facilitates attachment of functionalized molecules [25–28].

In this work, we used magnetic and gold nanoparticles (GNP) for enhancing the electrochemical signal of the DNA biosensor and increasing the sensitivity of the biosensor for HBV DNA detection. The use of 3-(trimethoxysilyl)-1-propanthiol (TMSPT) for the passivation of magnetic nanoparticles can increase the stability and reproducibility of the modified electrode. On the other hands, the free S-H group of TMSPT in the functionalized magnetic nanoparticles provides an enhanced loading interface for the gold nanoparticles and probe HBV ss-DNA. The proposed electrochemical DNA biosensor exhibited excellent sensitivity, good reproducibility and selectivity for determination trace amount of HBV DNA. These superior features can be related to unique synergism between magnetic and gold nanoparticles in the ss-DNA immobilization and also the high sensitivity of EIS technique. The promising performance of the developed DNA electrochemical biosensor makes this methodological study and application attractive in the HBV-DNA analysis.

2. Experimental

2.1. Materials

Potassium monohydrogen phosphate (K_2HPO_4), potassium dihydrogen phosphate (KH_2PO_4), potassium ferrocyanide [$K_4Fe(CN)_6$], potassium ferricyanide [$K_3Fe(CN)_6$], $FeCl_3 \cdot 6H_2O$, $FeCl_2 \cdot 4H_2O$, and ammonia solution were prepared from the Merck Company (Germany). All the DNA oligonucleotides used in this study were obtained from the Aminsan Company (Iran) with the following sequence:

HBV Probe (S1): S-H-5′- GAGGAGTTGGGGGAGCACATT-3′.

Complementary HBV DNA (S2): 5′-AATGTGCTCCCCCAACTCCTC-3′.
Three base mismatched DNA (S3): 5′-AGTGTGCTCTCCCAACTCCGC-3′.
Non-complementary DNA (S4): 5′-CACCTCAACCCCCTCGTGTAA-3′.

All oligonucleotides were dissolved in 0.1 M Phosphate buffer solutions (PBS) (pH 7.0) and were kept in the refrigerator at 4 °C. Phosphate buffer solutions (0.1 M) were prepared from KH_2PO_4 and K_2HPO_4. All other chemicals were of analytical reagent grade, and double distilled water (DDW) was used throughout.

2.2. Instruments

Electrochemical experiments, including cyclic voltammetry (CV), differential pulse voltammetry (DPV), and electrochemical impedance spectroscopy (EIS) were carried out with an Autolab 302 N electrochemical workstation (Metrohm-The Netherlands). The three-electrode system was composed of a platinum electrode as auxiliary (Azar electrode, Iran), an Ag/AgCl (saturated KCl) as a reference electrode (Azar electrode, Iran), and an unmodified/modified carbon paste as working electrode. The morphologies of the synthesized and modified magnetic nanoparticles were characterized with a JEM 1200 EXII transmission electron microscope (JOEL company-USA). A Shimadzu XRD-6000 X-ray diffractometer (Japan) with Cu-Kα radiation (wavelength = 0.154 nm) was used for powder X-ray diffraction (XRD) measurement. The powder was packed in the glass sample holder and the XRD patterns were collected between $10° < 2\theta < 90°$ with dwell time of 2 s and a step size of 0.02°. Fourier transform infrared (FT-IR) spectra were recorded on a Nicolet Magna-IR 550 spectrometer (USA) in the region of 4000–400 cm^{-1} with 4 cm^{-1} resolution.

2.3. Preparation of bare and functionalized magnetic nanoparticles

The magnetic nanoparticles (MNP) were prepared according to our previous works [29,30]. Briefly, 11.68 g of $FeCl_3 \cdot 6H_2O$ and 4.3 g $FeCl_2 \cdot 4H_2O$ were dissolved in 200 mL deionized water under nitrogen atmosphere with a vigorous stirring at 80 °C. Then, 45 mL of aqueous ammonia solution (25%) was added, and the color of the solution turned from dark orange to black immediately. The precipitates were washed three times with deionized water and twice with 0.02 M sodium chloride. The prepared magnetite suspension was placed in 250 mL round flask and was allowed to settle. For preparation of TMSPT coated magnetic nanoparticles (MNP/TMSPT), the supernatant was removed, and 80 mL aqueous solution of TMSPT 10% v/v and 60 mL of glycerol were added, respectively. The pH of the suspension was adjusted to 4.6 using glacial acetic acid, and the mixture was then stirred at 90 °C for 2 h under a nitrogen atmosphere. After cooling to room temperature, the suspension was sequentially washed with deionized water, methanol, and deionized water. Finally, the MNP/TMSPT composite was stored in deionized water at a concentration of 40 g/L.

Gold nanoparticle modified MNP (MNP/GNP) or gold nanoparticle modified MNP/TMST (MNP/TMSPT/GNP) were prepared according to literature [31,32]. Briefly, 0.229 g of sodium citrate was dissolved in 100 mL of DDW, and the solution was heated to 99 °C under vigorous stirring. Then 1 mL of the prepared MNP or MNP/TMSPT suspension was added to the solution. Finally, 5 mL of 10 mM $HAuCl_4$ was slightly added to the solution, the water bath was removed, and the suspension was stirred for 15 min. The solid was removed again by a magnet and was rinsed with deionized water as the claret-red suspension was cooled down to the ambient temperature. Then, MNP/GNP or MNP/

TMSPT/GNP suspensions were prepared by dispersing the solid in 20 mL water, which was kept at 4 °C.

2.4. Preparation of gold nanoparticles

Approximately, 30 nm diameter gold nanoparticles were prepared by the citrate reduction of $HAuCl_4$ [33]. All glassware was cleaned in aqua regia (3 parts HCl, 1 part HNO_3), were rinsed with DDW, and were dried prior to use. An aqueous solution of $HAuCl_4$ (0.01% w/v, 30 ml) was poured into the beaker and was heated until the temperature of the solution reached to 85 °C. Afterward, 1 ml of a 1% (w/v) trisodium citrate aqueous solution was added quickly, which resulted in a change in solution color from pale yellow to pale black. After another 10 min of stirring, the solution color shifted to deep red. After the appearance of red color, the solution was stirred for an additional 30 min and was allowed to cool to room temperature. Finally, the prepared gold nanoparticles were stored in dark glass at 4 °C.

2.5. Preparation of unmodified/modified carbon paste electrodes

Bare carbon paste electrodes (CPE) were prepared according to a previous work [34] by mixing 238 mg of graphite powder with 132 mg of paraffin oil with a mortar and pestle. Then, the paste was taken into a polyethylene tube (10 mm diameter) which has a 10 T magnet (2 mm height) inserted inside it and at the tip of which had been cut off previously. Electrical contact with the paste was established via inserting a copper wire through flank. Bare carbon paste electrode was immersed in a basic solution of magnetic nanoparticles containing 3.75 mM NaOH for 4 h. The accumulated magnetic nanoparticles on the CPE surface was washed with DDW and this electrode was named as CPE/MNP.

In comparative studies, CPE/MNP/TMSPT/GNP and CPE/MNP/GNP were prepared as mentioned above by inserting the bare CPE electrodes into the prepared MNP/TMSPT/GNP and MNP/GNP suspensions. Gold nanoparticles modified carbon paste electrode (CPE/GNP) was also prepared by mixing appropriate amounts of graphite powder, paraffin oil, and gold nanoparticles.

2.6. Preparation of real samples

Urine samples were stored in a refrigerator at 4 °C immediately after collection. 10 mL of the sample was centrifuged for 20 min at 1000 rpm. The supernatant was filtered using a 0.45 mm filter and was diluted four times with the phosphate buffer solution (pH 7.0). The solution was transferred into a voltammetric cell without any further pretreatment, and standard addition method was applied for the determination of HBV-DNA contents.

In order to precipitate proteins in the plasma samples, 1.0 mL of the sample was treated with 20 mL $HClO_4$, 20% v/v. Then, the mixture was vortexed for a further 30 s and was centrifuged at 1000 rpm for 20 min. The solution was diluted five times with water and was transferred into a voltammetric cell. Once more, the standard addition method was applied for the determination of HBV-DNA contents.

2.7. Immobilization of thiolated HBV probe DNA

Three thiolated HBV probe DNA immobilized electrodes were prepared by immersing CPE/MNP/TMSPT/GNP, CPE/MNP/GNP, and CPE/GNP electrodes in a 10^{-8} M PBS solution of S-H modified HBV probe DNA (pH 7.0) for 6 h. Afterward, the electrode surfaces were incubated in the mercaptohexanol (MCH) solution for 30 min. This process would produce a self-assembly well-aligned monolayer (SAM) of thiolated oligonucleotide. Then, the electrode surfaces were rinsed thoroughly with DDW to remove physically adsorbed S-H HBV probe DNA and the obtained modified electrodes were denoted as CPE/MNP/TMSPT/GNP/ss-DNA, CPE/MNP/GNP/ss-DNA, and CPE/GNP/ss-DNA, respectively.

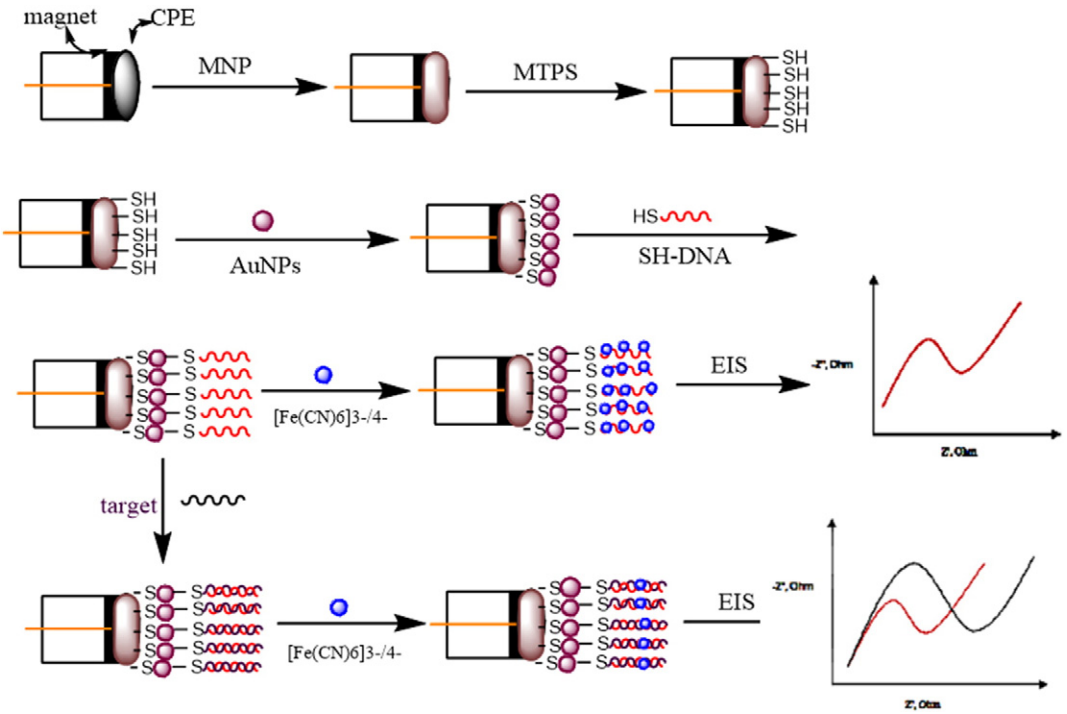

Fig. 1. Schematic illustration of the fabrication steps of the electrochemical DNA biosensor.

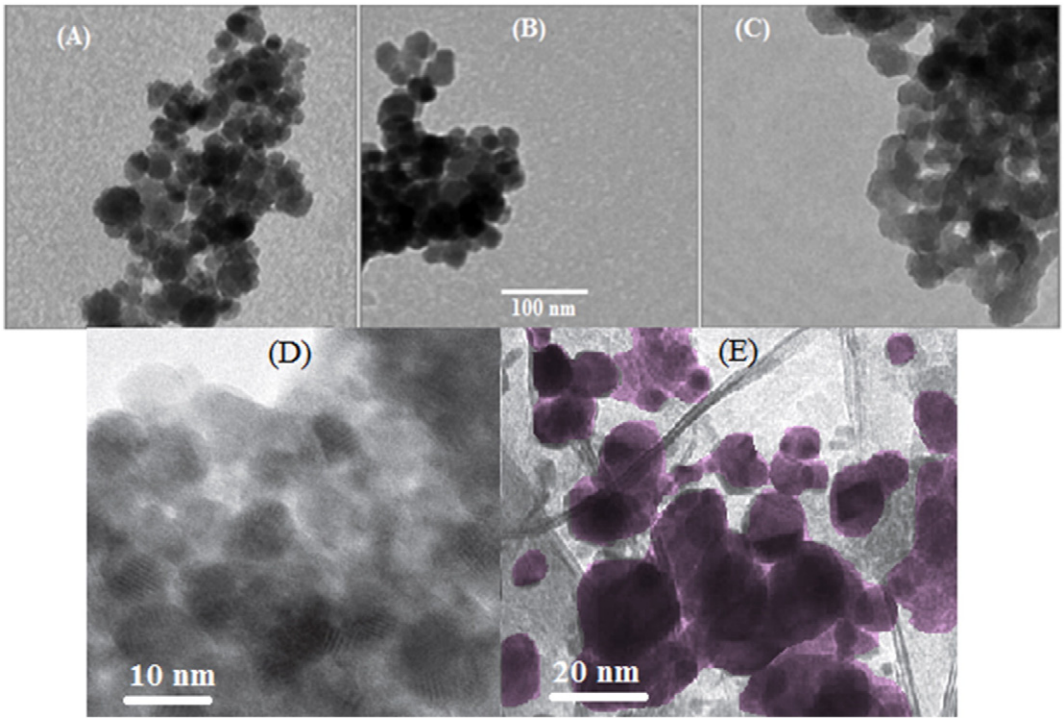

Fig. 2. TEM images of GNP (A), MNP/GNP (B), and MNP/TMSPT/GNP (C) after the immobilization of HBV probe DNA. TEM micrographs of (D) uncoated and (E) gold coated magnetic nanoparticles.

2.8. Electrochemical measurements

The modified electrodes obtained during the biosensor fabrication were electrochemically characterized using EIS and CV methods based on our previous work [35]. CV measurements were performed using 0.1 M PBS (pH 7.0) solution as the supporting solution, 5 mM $K_4Fe(CN)_6$ and 0.1 M KNO_3. EIS measurements were performed in 5.0 mM $K_3Fe(CN)_6/K_4Fe(CN)_6$ (1:1) mixture containing 0.1 M KNO_3.

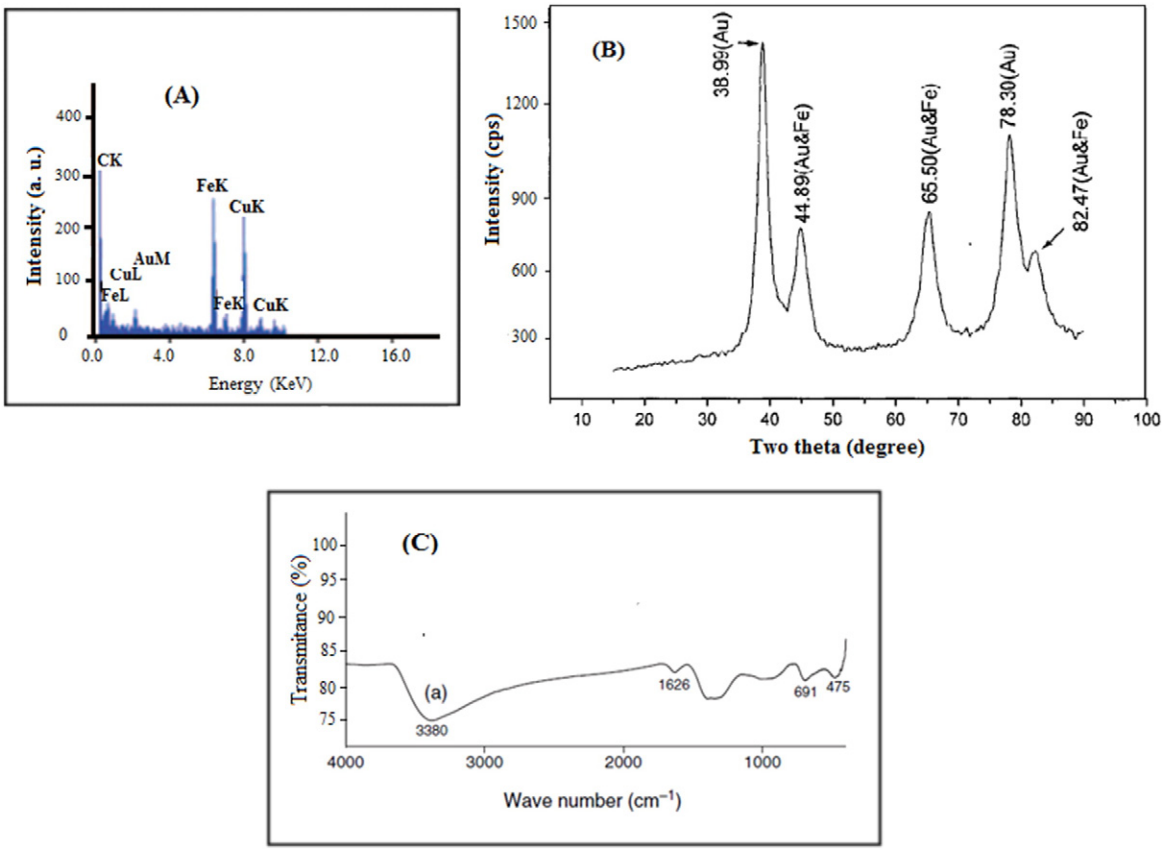

Fig. 3. EDX spectrum (A), XRD pattern (B), and FT-IR of gold coated magnetic nanoparticles (C).

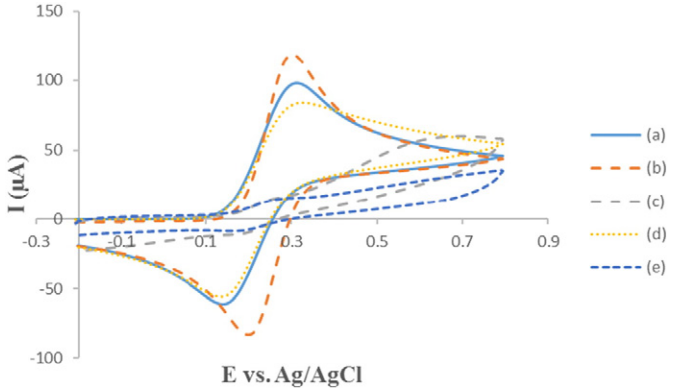

Fig. 4. Cyclic voltammograms obtained at the bare CPE (a), CPE/MNP (b), CPE/MNP/TMSPT (c), CPE/MNP/TMSPT/GNP (d) and CPE/MNP/TMSPT/GNP/S_1 (e) electrodes in a 5 mM $K_4[Fe(CN)_6]$ solution containing 0.1 M KNO_3, with a scan rate of 50 mV/s.

The EIS measurements were performed with the frequency range from 10^5 to 0.1 Hz at the formal potential of the system, E° = 0.182 V.

3. Result and discussion

For the first time a modified carbon paste electrode with both gold and magnetic nanoparticle and a thiol modified hepatitis B virus probe DNA were used for designing a highly sensitive and selective hepatitis B virus DNA biosensor. Our result showed that both gold and magnetic nanoparticles had a great effect on the response of a DNA biosensor. Gold and magnetic nanoparticles can increase the electrode surface area and accelerates the electron transfer on the electrode surface. The whole DNA biosensor fabrication process was schematically presented in Fig. 1.

3.1. Characterization the immobilization of probe DNA

The media obtained after immobilization of ss-DNA onto the magnetic nanoparticles were separated using a magnetic separator and were washed with the immobilization buffer to remove the unbound oligonucleotides. The remaining modified magnetic nanoparticle-ss DNA conjugates were diluted in the immobilization buffer, and the mixture was used for TEM analysis. TEM images of the GNP, MNP/GNP, and MNP/TMSPT/GNP after DNA immobilization are shown in Fig. 2A-C, respectively. It should be noted that the functionalization step tends to increase the particle size slightly. Consequently, GNP/ss-DNA and MNP/GNP/ss-DNA were smaller than MNP/TMSPT/GNP/ss-DNA. MNP/GNP/ss-DNA was slightly larger than GNP/ss-DNA. This difference in size could have resulted from the gold nanoparticles coating on the magnetite nanoparticles.

The size and morphology of individual particles can also be observed in the TEM micrographs (Fig. 2D-E). As can be seen from this figure, nanoparticles were equiaxed for both coated and uncoated samples. Uncoated particles have an average size of 50 nm and coated particles have an average size of 78 nm.

The EDX spectrum of gold coated magnetic nanoparticles (Fig. 3A) was generated with an electron nano-probe (~20 nm in diameter) revealed both iron (0.034, 6.24, and 6.99 keV) and gold (2.08 keV) peaks. No oxygen peak was found, suggesting that there was negligible oxidation of iron. The peaks corresponding to carbon and copper arise from the sample holder.

A representative XRD pattern of the gold coated magnetic nanoparticles is shown in Fig. 3B. The diffraction peaks at 2θ° = 38.99°, 44.89°, 65.50°, 78.30°, and 82.47° are attributed to gold, which can be indexed to 111, 200, 220, 311, and 222 lattice planes of gold in a cubic phase, respectively. The pattern of α-iron is hidden under the pattern of gold due to the overlapping of their diffraction peaks at 2θ = 44.8°, 65.5°, and 82.5°.

Fig. 3C shows FT-IR spectra of gold nanoparticles coated magnetic nanoparticles. The characteristic absorption peaks at 475 and 679 cm^{-1} are attributed to the Fe–O structure and are considered as an indication of the ferrite formation. The observed peaks at 3380 cm^{-1} (H–O stretching), 1626 cm^{-1} (H–O–H bending) are due to adsorbed water on the surface of nanoparticles.

3.2. Optimization of DNA assay conditions

A series of ss-DNA-modified electrodes with different concentrations of probe DNA were prepared. During the performed experiments for developing HBV DNA biosensor, it was found that the surface concentration of immobilized DNA probe influenced on the signal of the

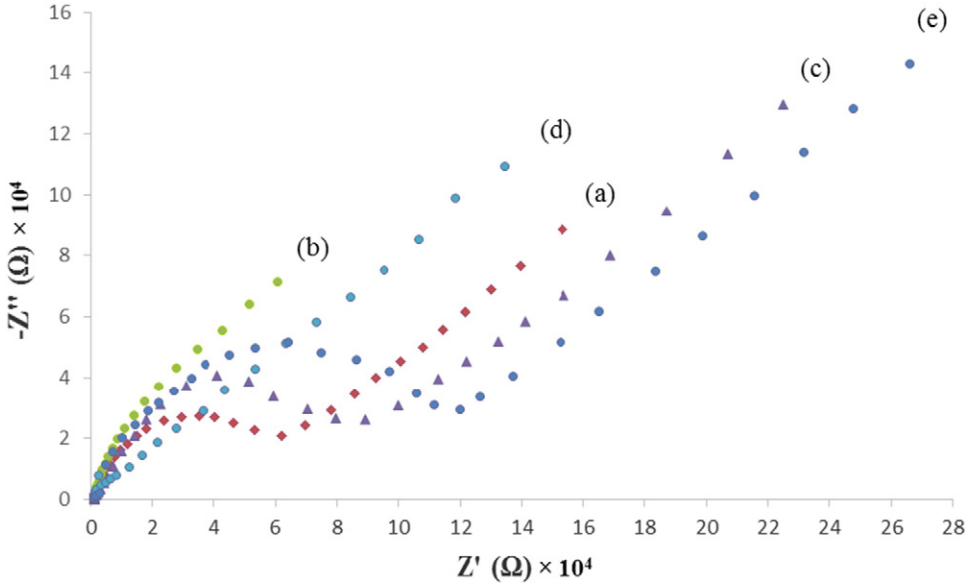

Fig. 5. The Nyquist plots of the bare CPE (a), CPE/MNP (b), CPE/MNP/TMSPT (c), CPE/MNP/TMPT/GNP (d) and CPE/MNP/TMSPT/GNP/S1 (e) in 5.0 mM $[K_3Fe(CN)_6]/[K_4Fe(CN)_6]$ (1:1) solution containing 0.1 M KNO_3 at the potential of 0.182 V with the frequency ranged from 0.1 Hz to 100 kHz. The concentration of DNA was 1.0×10^{-8} mol/L. "−Z" and "Z" refer to imaginary and real impedance, respectively.

biosensor. To get maximum signal response, surface concentration of probe DNA was optimized, using different concentrations of probe DNA in the immobilization process on the surface of MNP/TMSPT/GNP electrode. It was observed that the highest signal of DNA biosensor was observed when the probe concentration was 10^{-8} M. After immobilization of higher probe DNA concentration the signal of the developed biosensor decreased. It clearly indicated that the control of ss-DNA concentration was essential for the sensitivity. The results showed that the ideal probe concentration was 10^{-8} M. Electrochemical signal of a DNA biosensor is a sensitive function of the surface density of immobilized probe DNA. The different surface densities were obtained by controlling the concentration of probe DNA employed during the fabrication process. Low-density (8.6×10^{12} molecules/cm^2) surfaces were obtained by incubation of electrodes with 0.01 μM of probe DNA. Medium-density (9.3×10^{13} molecules/cm^2) and high-density (7.1×10^{14} molecules/cm^2) surfaces were prepared by incubation of electrodes with 0.1 and 1 μM of probe DNA, respectively. The DNA surface densities were quantitatively measured as previously described procedure [36].

In our experiments, highest difference in the R_{CT} (charge transfer resistance) after probe DNA immobilization was observed at low density of probe DNA. The difference in the R_{CT} decreased along with surface density increasing, with the highest signal at low-density surfaces and lowest signal at high-density surfaces. This clearly showed that control of DNA surface density was essential for sensitivity improvement, and that low-density DNA probes were optimal for high-sensitivity DNA detection.

3.3. Electrochemical characterization of modified electrodes

Fig. 4 shows the cyclic voltammograms of different modified electrodes in 0.1 M PBS (pH 7.0) solution containing 1.0 mM $[Fe(CN)_6]^{4-}$ and 0.1 M KNO_3. It can be seen that the CPE electrode (curve a) gave a pair of redox peaks with approximately large peak-to-peak separation. These peaks could be definitely attributed to the redox behaviors of $[Fe(CN)_6]^{4-}$ on the bare CPE. After the MNP modification, the oxidation response increased and ΔEp (difference between anodic and cathodic potentials) decreased (curve b), which

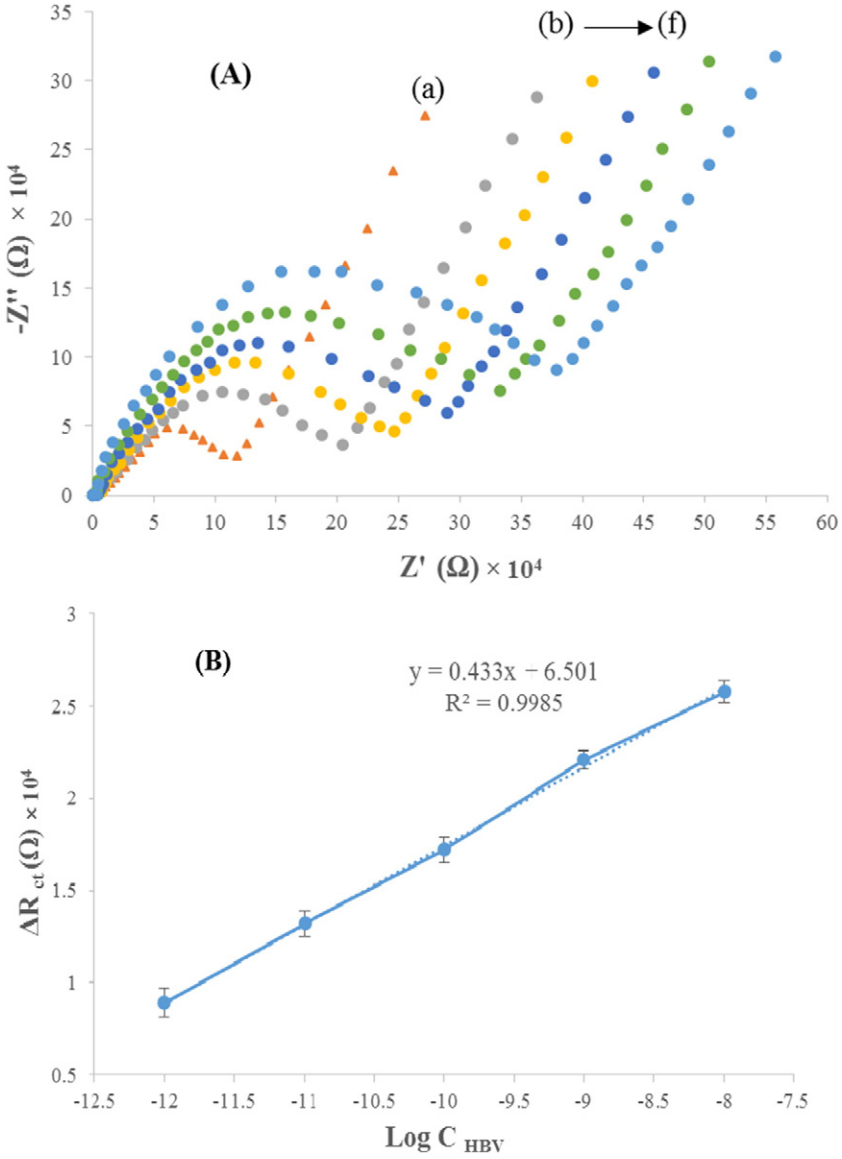

Fig. 6. EISs of $[K_3Fe(CN)_6]/[K_4Fe(CN)_6]$ on the CPE/MNP/TMSPT/GNP for 10^{-8} M probe ss-DNA (a) and after its hybridization with different concentration of the target sequence in a 0.1 M PBS (pH 7.0) with 20 mM NaCl. Target concentration: (b) 1.0×10^{-12}, (c) 1.0×10^{-11}, (d) 1.0×10^{-10}, (e) 1.0×10^{-9} and (f) 1.0×10^{-8} M. (B) Calibration curve illustrating the variation in R_{CT} with concentration of complementary target.

Table 1
Comparative study between some characteristics of modified carbon paste electrodes.

Electrode name	Concentration range (M)	Detection limit (M)	R^2
CPE/MNP/TMSPT/GNP/ss-DNA	8.3×10^{-13}–6.4×10^{-7}	3.1×10^{-13}	0.9985
CPE/MNP/GNP/ss-DNA	2.9×10^{-12}–5.8×10^{-8}	7.9×10^{-12}	0.9954
CPE/GNP/ss-DNA	4.2×10^{-10}–5.6×10^{-7}	9.4×10^{-10}	0.9963

Table 2
Within-day and between-day studies on the determination of HBV DNA.

HBV DNA added (M)	Within day		Between day	
	HBV DNA found (M)	RSD%	HBV DNA found (M)	RSD%
1.00×10^{-9}	9.84×10^{-10}	4.4 (±0.1)	9.51×10^{-10}	4.8 (±0.2)
1.00×10^{-10}	9.91×10^{-11}	4.3 (±0.1)	9.77×10^{-11}	4.6 (±0.2)
1.00×10^{-11}	9.74×10^{-12}	4.9 (±0.2)	9.64×10^{-12}	5.1 (±0.3)

was due to the good catalytical ability and excellent conductivity of MNP. The current responses of $[Fe(CN)_6]^{4-}$ at CPE/MNP/TMSPT (curve c) decreased compared with that at CPE/MNP, which indicated that the TMSPT as an insulating layer, can lower the electron transfer rate of $[Fe(CN)_6]^{4-}$. With the immobilization of gold nanoparticles on the CPE/MNP/TMSPT electrode surface (curve d) the electron transfer rate of $[Fe(CN)_6]^{4-}$ improved. This showed that gold nanoparticles successfully immobilized and facilitated the required conduction at the electrode surface. After immobilization of ss-DNA on the CPE/MNP/TMSPT/GNP electrode (curve e) the current responses decreased. The decrease in peak current and increase in peak potentials of $[Fe(CN)_6]^{4-}$ redox reaction at the probe immobilized electrode was observed due to its insulating manner on the electrode surface and the repulsive electrostatic interactions between negatively charged DNA and ferricyanide ions.

The surface areas of different modified electrodes were calculated using Randles–Sevcik equation:

$$I_{pc} = \left(2.69 \times 10^5\right)\ n^{3/2} A D^{1/2} C * v^{1/2},$$

where I_{pc} is the reduction peak current (A), n is the electron transfer number, A is the electroactive surface area (cm^2), D is the diffusion coefficient of $K_4[Fe(CN)_6]$ in the solution ($cm^2\ s^{-1}$), C* is the concentration of $K_4[Fe(CN)_6]$ (mol cm^{-3}), and v is the scan rate ($V\ s^{-1}$). By exploring the redox peak current with the scan rate, the average electroactive area of bare CPE, CPE/GNP, CPE/MNP/GNP, CPE/MNP/TMSPT/GNP electrodes were calculated 0.271, 0.314, 364, and 0.399 cm^2, respectively. These results indicated that the presence of gold and magnetic nanoparticles improved the effective area of the electrode surface greatly.

EIS is a useful method for studying the surface properties of the modified electrode [37]. In Nyquist diagram, the observed semicircle portion at high frequencies corresponds to the electron transfer limiting process. The electron transfer resistance, R_{CT}, can be directly measured as the semicircle diameter. As can be observed in Fig. 5, when MNP and GNP were modified on the surface of CPE and CPE/MNP/TMSPT, respectively, the semicircles for CPE/MNP (curve b) and CPE/MNP/TMSPT/GNP (curve d) dramatically decreased as compared to CPE (a) and CPE/MNP/TMSPT (c). This observation indicated that both MNP and GNP promoted the charge transfer. For CPE/MNP/TMSPT (c), the semicircle surprisingly increased as compared to the CPE/MNP, suggested that TMSPT acted as an insulating layer which made the interfacial charge transfer difficult and TMSPT repelled the access of $[Fe(CN)_6]^{4-}$ to the electrode surface for electron communication. After the HBV ss-DNA immobilization onto CPE/MNP/TMSPT/GNP, an increase in semicircle for CPE/MNP/TMSPT/GNP/ss-DNA (curve e) was observed because of repulsion between negative charges of DNA and $[Fe(CN)_6]^{4-}$.

3.4. Sensitivity of the developed DNA biosensor

Under the optimal conditions, the analytical performance of the CPE/MNP/TMSPT/GNP was investigated using the immobilized probe DNA after hybridization with different concentrations of target HBV DNA. Fig. 6 shows EIS of $[Fe(CN)6]^{3-/4-}$ at the CPE/MNP/TMSPT/GNP/ss-DNA before and after hybridization with the different concentration of target oligonucleotides. As can be seen from Fig. 6, when the complementary HBV DNA concentrations were increased in the solution, the ΔR_{CT} increased, and the values of the ΔR_{CT} were linear with the logarithm of HBV DNA concentrations from 8.3 (±0.1) × 10^{-13} to 6.4 (±0.2) × 10^{-7} M. The regression equation was $\Delta R_{CT} = 0.433 \mathrm{Log}\ C_{HBV} + 6.501$ (unit of C is M), with a detection limit of 3.1 (±0.1) × 10^{-13} M (S/N = 3). The regression coefficient (R^2) of the calibration curve was 0.9985.

In a comparative study, CPE/GNP and CPE/MNP/GNP electrodes were immobilized by probe DNA and were incubated with different concentrations of HBV DNA for the hybridization efficiency testing, and results are shown in Table 1.

As can be seen from Table 1, the best efficiency (wide concentration range and low detection limit) was achieved at the CPE/MNP/TMSPT/GNP/ss-DNA, CPE/MNP/GNP/ss-DNA, and CPE/GNP/ss-DNA electrodes, respectively. Hybridization efficiency for CPE/MNP/GNP/ss-DNA was better than CPE/GNP/ss-DNA, indicated that the synergistic effect of

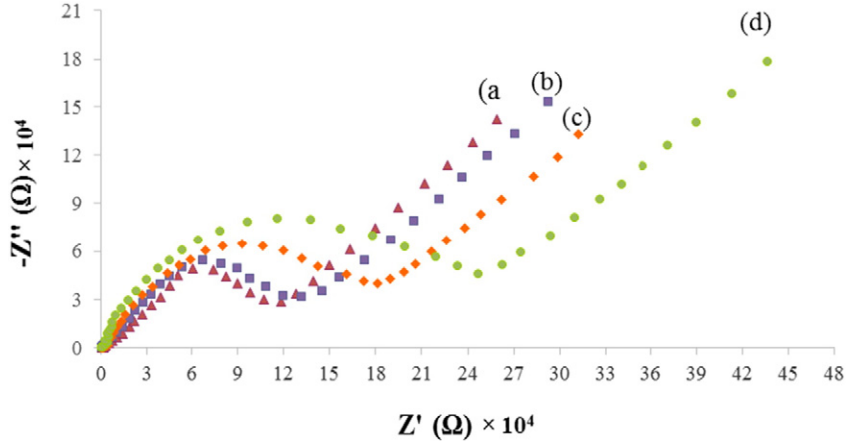

Fig. 7. EIS recorded at CPE/MNP/TMSPT/GNP/ss-DNA (a) and after its hybridization with non-complementary oligonucleotides (b), three-base mismatched DNA (c), and complementary DNA (d). The concentrations of probe DNA was 10^{-8} M and concentration of other oligonucleotides sequences were 10^{-12} M.

Table 3
Analytical results of spiked urine and blood plasma samples[a].

Sample	Added HBV DNA (M)	Found HBV DNA(M)	Recovery (%)
Urine	1.00×10^{-10}	$9.72\ (\pm 0.05) \times 10^{-11}$	97.2
	1.00×10^{-9}	$1.03\ (\pm 0.06) \times 10^{-9}$	103.0
Blood plasma	1.00×10^{-10}	$1.04\ (\pm 0.07) \times 10^{-10}$	104.0
	1.00×10^{-9}	$1.05\ (\pm 0.09) \times 10^{-9}$	105.0

[a] Values in parentheses are RSDs based on three replicates.

magnetite and gold nanoparticles in the MNP/GNP was more favorable to improve the immobilization amount of ss-DNA on the electrode surface. This synergism is due to properties of magnetic nanoparticles such as their influence on increasing the surface and their magnetic feature and also properties of gold nanoparticles such as increasing the electrode surface area and their strong covalent interaction with thiolated HBV ss-DNA. Indeed, the presence of magnetite and gold nanoparticles with together have an excellent effect of capturing the target HBV DNA in the solution. However, the best result was obtained with the CPE/MNP/TMSPT/GNP/ss-DNA, because of the TMSPT effect on the better loading of gold nanoparticles onto the magnetite nanoparticles modified electrode that improves reproducibility and stability of magnetic nanoparticle modified electrode.

3.5. Specificity of the developed DNA biosensor

The hybridization specificity of the developed biosensor was investigated by CPE/MNP/TMSPT/GNP/ss-DNA electrode as a capture probe to hybridize with various DNA sequences. Fig. 7 shows the obtained EIS of CPE/MNP/TMSPT/GNP/ss-DNA before (curve a) and after hybridization with fully complementary HBV DNA (S2, curve d), three-bases mismatched (S3, curve c), and non-complementary (S5, curve b) sequences. It was clear that the value of R_{CT} in curve b was very close to that in the curve a, suggesting that the states of these two electrodes were similar, i.e., S5 has not been captured in the surface by CPE/MNP/TMSPT/GNP/ss-DNA via a hybridization reaction. While after hybridization with fully complementary sequences of S2, the obtained R_{CT} value increased extremely because of the formation of the intact duplex (curve d).

Moreover, the specificity of the biosensor was also assessed by detecting the target sequences with the three base-mismatched DNA. When three-bases mismatched target sequence was hybridized (curve c), the decrease in the R_{CT} value was very smaller than target sequence, suggesting that the developed biosensor had high specificity to recognize the target sequences with the different complementary degree.

3.6. Repeatability, stability and regeneration of the developed biosensor

The repeatability of the prepared DNA biosensor was estimated by making repetitive hybridizations with the 10^{-9} M of the target HBV DNA. The relative standard deviation (RSD) based on five measurements for the target HBV DNA with the same modified.

CPE/MNP/TMSPT/GNP/ss-DNA electrode was 4.1 (±0.2) %. In addition, the impedance signal of 10^{-9} M almost remained unchanged after the biosensors were stored in the PBS buffer for at least 7 days, demonstrated that the present method for DNA determination had good repeatability and stability. The impedimetric DNA biosensor demonstrated here was reusable for repeated detection of DNA hybridization. The regeneration could be simply performed by first immersing the CPE/MNP/TMSPT/GNP/S1–S2 electrode into 0.1 M NaOH solution for 120 s and then challenging the electrode in the hybridization buffer containing 10^{-9} M target HBV DNA. By doing so, the sensor signal was almost recovered to the original value.

3.7. Within-day and between-day precision study

To ascertain the ruggedness of the method, three replicate determinations at different concentration levels of HBV DNA were carried out. The results showed that, the within-day relative standard deviation values were 4.3 (±0.1)–4.9 (±0.2) %. The between-day relative standard deviations for different concentrations of HBV DNA were obtained from the average of five determinations carried out over a period of three days were 4.6 (±0.2)–5.1 (±0.3) %. These results indicated that, the recommended method had an advantage of excellent reproducibility in both within-day and between-day precision as shown in Table 2.

3.8. Analytical application

Unfortunately, we don't access to a hepatitis patient. Therefore, based on our previous work [38], **t**he recovery experiments were performed only for accuracy assessment. In order to investigate the accuracy of the method, urine and blood plasma samples were analyzed to determine their HBV-DNA contents. In this regard, the samples were prepared as described in the sample preparation section. For blood plasma and urine samples, the concentrations of HBV-DNA in the samples were determined. Then, known concentrations of HBV-DNA were added into the same sample volume before their being centrifuged. After sample preparation, the HBV-DNA in the spiked samples was measured simultaneously. The data obtained with the proposed biosensor for spiked HBV-DNA in urine and blood plasma samples are presented in Table 3. The results showed that the determination of HBV-DNA was satisfactorily accurate.

3.9. Comparison study

The analytical performances of the designed DNA biosensor were compared with other previously reported electrochemical DNA biosensors and the results were summarized in Table 4. It can be seen that the lower detection limit, and a wide detection range of the target ss-DNA sequences can be achieved with the proposed biosensor. The high sensitivity of proposed DNA biosensor can be related to effective immobilization of probe DNA onto the electrode surface because the synergistic effect of magnetite and gold nanoparticles that catalyst the electrode reaction and increase the surface area of carbon paste electrode and hence increase the loading of DNA amount and improve the sensitivity of the biosensor.

Table 4
Comparison of the analytical parameters with other electrochemical DNA biosensor.

References	Immobilization technique	Detection method	Linear range (M)	Detection limit (M)
[39]	Electrostatic immobilization onto ZnO nanostructure	DPV	1.0×10^{-12}–1.0×10^{-6}	1.0×10^{-12}
[40]	Covalent immobilization by direct coupling of sol–gel and self-assembly technology	DPV	2.5×10^{-9}–5.0×10^{-7}	8.6×10^{-10}
[41]	Adsorption of the nanogold/ZrO_2 film	DPV	1.0×10^{-10}–5.0×10^{-6}	3.1×10^{-11}
[42]	Assembled the SH-DNA onto the nanogold	DPV	1.5×10^{-10}–4.1×10^{-8}	1.0×10^{-10}
[43]	Assembled the SH-DNA onto sol–gel network based nanogold	EIS	1.0×10^{-8}–1.0×10^{-6}	5.0×10^{-9}
[44]	Immobilization by gold nanoparticles and grapheme	DPV	2.5×10^{-11}–1.3×10^{-9}	8.33×10^{-12}
This work	Covalent immobilization using magnetite and gold nanoparticles modified paste electrode	EIS	8.3×10^{-13}–6.4×10^{-7}	3.1×10^{-13}

4. Conclusion

The presence of magnetite and gold nanoparticles on the carbon paste electrode surface had synergistic effects on the immobilization of the HBV ss-DNA probe. This synergistic effect can enlarge the surface area and improve charge transport characteristics of the electrode and increases the ss-DNA loading quantity and enhances the detection sensitivity of the modified electrode for DNA hybridization. The DNA electrochemical sensor was successfully applied to the detection of the HBV short sequence with a dynamic concentration range from 8.3 $(\pm 0.1) \times 10^{-13}$ to 6.4 $(\pm 0.2) \times 10^{-7}$ M and the detection limit of 3.1 $(\pm 0.1) \times 10^{-13}$ M (3S/m) (where S is the standard deviation of the blank solution (n=5) and m is the slope of calibration curve). The proposed impedimetric biosensor was also applied to the determination of HBV DNA in the urine and blood plasma samples. The results indicated that the biosensor showed the advantages such as simple preparation procedure, high selectivity, low cost, fast response, wide concentration range, and low detection limit.

References

[1] A.C.M. Boon, A.M.F. French, D.M. Fleming, M.C. Zambon, J. Med. Virol. 65 (2001) 163–170.
[2] A. Voller, A. Bartlett, D.E. Bidwell, M.F. Clark, A.N. Adams, J. Gen. Virol. 33 (1966) 165–167.
[3] M.H. Mashhadizadeh, R.P. Talemi, Chin. Chem. Lett. 26 (2015) 160–166.
[4] B.N. Chandrashekar, B.E. Kumara Swamy, Anal. Methods 4 (2012) 849–854.
[5] M.K. Dey, A.K. Satpati, S. Sahoo, R. Kameswaran, A.V.R. Reddy, T. Mukherjee, Anal. Methods 3 (2011) 2540–2546.
[6] M.K. Dey, A.K. Satpati, V.R. Reddy, Anal. Methods 6 (2014) 5207–5213.
[7] P. Snevajsova, L. Tison, I. Brozkova, J. Vytrasova, R. Metelka, K. Vytras, Electrochem. Commun. 12 (2010) 106–112.
[8] M.H. Mashhadizadeh, R.P. Talemi, A. Shokravi, M. Kamali, Anal. Methods 4 (2012) 742–747.
[9] F. Bedioui, N. Villeneuve, Electroanalysis 15 (2003) 5–18.
[10] S. Tajik, M.A. Taher, H. Beitollahi, M.T. Mahani, Talanta 134 (2015) 60–64.
[11] S. Tajik, M.A. Taher, H. Beitollahi, J. Electroanal. Chem. 720 (2014) 134–138.
[12] K. Liu, J. Zhang, G. Yang, C. Wang, J.J. Zhu, Electrochem. Commun. 12 (2010) 402–405.
[13] J.P. Hart, S.A. Wring, Trends Anal. Chem. 16 (1997) 89–103.
[14] K. Rajeshwar, J.G. Ibanez, G.M. Swain, J. Appl. Electrochem. 24 (1994) 1077–1091.
[15] A.D. Chowdhury, R. Gangopadhyay, A. De, Sensors Actuators B Chem. 190 (2014) 348–356.
[16] P.S. Petrou, S.E. Kakabakos, K. Misiakos, Int. J. Nanotechnol. 6 (2009) 4–17.
[17] T.G. Drummond, M.G. Hill, J.K. Barton, Nat. Biotechnol. 21 (2003) 1192–1199.
[18] Y. Wang, C. Li, X. Li, Y. Li, H.B. Kraatz, Anal. Chem. 80 (2008) 2255–2260.
[19] J. Kafka, O. Pänke, B. Abendroth, F.A. Lisdat, Electrochim. Acta 53 (2008) 7467–7474.
[20] J. Huang, G. Yang, W. Meng, L. Wu, A. Zhu, X. Jiao, Biosens. Bioelectron. 40 (2009) 893–896.
[21] A.P. Alivisatos, Science 271 (1966) 933–938.
[22] S. Sun, C.B. Murray, D. Weller, L. Folks, A. Moser, Science 287 (2000) 1989–1995.
[23] X.M. Lin, C.M. Sorensen, K.J. Klabunde, G.C. Hadjipanayis, *Langmuir* 14 (1998) 7140–7148.
[24] F. Bodker, S. Morup, S. Linderoth, Phys. Rev. Lett. 72 (1994) 282–289.
[25] C. Pathmamnoharan, A.P. Philipse, J. Colloid Interface Sci. 205 (1998) 340–346.
[26] M. Klotz, A. Ayral, C. Guizard, C. Menager, V. Cabuil, J. Colloid Interface Sci. 220 (1999) 357–364.
[27] N.L. Rosi, C.A. Mirkin, Chem. Rev. 105 (2005) 1547–1562.
[28] C. Minard-Basquin, R. Kugler, N.N. Matsuzawa, A. Yasuda, Nanobiotechnology 152 (2005) 97–103.
[29] M.H. Mashhadizadeh, Z. Karami, J. Hazard. Mater. 190 (2011) 1023–1029.
[30] M.H. Mashhadizadeh, R.P. Talemi, J. Iran Chem. Soc. 12 (2015) 1747–1756.
[31] G.K. Kouassi, P. Wang, S. Sreevatan, J. Irudayaraj, Biotechnol. Prog. 23 (2007) 1239–1244.
[32] G.K. Kouassi, J. Irudayaraj, Anal. Chem. 78 (2006) 3234–3241.
[33] M.H. Mashhadizadeh, R.P. Talemi, Spectrochim. Acta A 132 (2014) 403–409.
[34] M.H. Mashhadizadeh, R.P. Talemi, Anal. Chim. Acta 692 (2011) 109–115.
[35] M.H. Mashhadizadeh, R.P. Talemi, Talanta 131 (2015) 460–466.
[36] R. Lao, S. Song, H. Wu, L. Wang, Z. Zhang, L. He, C. Fan, Anal. Chem. 77 (2005) 6475–6480.
[37] L. Wang, X. Chen, X. Wang, X. Han, S. Liu, C. Zhao, Biosens. Bioelectron. 30 (2011) 151–157.
[38] M.H. Mashhadizadeh, R.P. Talemi, Anal. Methods 6 (2014) 8956–8964.
[39] M. Das, G. Sumana, R. Nagarajan, B.D. Malhotra, Thin Solid Films 519 (2010) 1196–1201.
[40] F. Li, W. Chen, S. Zhang, Biosens. Bioelectron. 24 (2008) 781–786.
[41] W. Zhang, T. Yang, C. Jiang, K. Jiao, Appl. Surf. Sci. 254 (2008) 4750–4756.
[42] J. Kang, X. Li, G. Wu, Z. Wang, X. Lu, Anal. Biochem. 364 (2007) 165–170.
[43] Y. Fu, R. Yuan, L. Xu, Y. Chai, X. Zhong, D. Tang, Biochem. Eng. J. 23 (2005) 37–44.
[44] S. Niu, J. Sun, C. Nan, J. Lin, Sensors Actuators B Chem. 176 (2013) 58–65.